Droughts, Pluvials, and Wet Season Timing across the Chao Phraya River Basin: a 254-Year Monthly Reconstruction from Tree Rings and δ^{18}O

Hung T.T. Nguyen[1], Stefano Galelli[1,2], Chenxi Xu[3,4], and Brendan M. Buckley[1]

[1]Lamont-Doherty Earth Observatory, Columbia University, New York, USA
[2]Pillar of Engineering Systems and Design, Singapore University of Technology and Design, Singapore
[3]Key Laboratory of Cenozoic Geology and Environment, Institute of Geology and Geophysics, Chinese Academy of Sciences, Beijing, China
[4]Chinese Academy of Sciences Center for Excellence in Life and Paleoenvironment, Beijing, China

Key Points:

- Monthly-resolved reconstructions of streamflow across the Chao Phraya River Basin are produced from tree rings and δ^{18}O.
- Droughts and pluvials across the Chao Phraya show both coherence and heterogeneity in time and space.
- The reconstruction reveals the spatiotemporal variability of wet season timing.

Corresponding author: Hung Nguyen, hnguyen@ldeo.columbia.edu

Abstract

Water system operations require subannual streamflow data—e.g., monthly or weekly—that are not readily achievable with conventional streamflow reconstructions from annual tree rings. This mismatch is particularly relevant to highly seasonal rivers such as Thailand's Chao Phraya. Here, we combine tree ring width and oxygen isotope (δ^{18}O) from Southeast Asia to produce 254-year, monthly-resolved reconstructions for all four major tributaries of the Chao Phraya. From the reconstructions, we derive subannual streamflow indices to examine past hydrological droughts and pluvials, and find coherence and heterogeneity in their histories. The monthly resolution reveals the spatiotemporal variability in wet season timing, caused by interactions between early summer typhoons, monsoon rains, catchment location, and topography. Monthly-resolved reconstructions, like the ones presented here, not only broaden our understanding of past hydroclimatic variability, but also provide data that are functional to water management and climate-risk analyses, a significant improvement over annual reconstructions.

Plain Language Summary

Long records of river discharge, reconstructed from tree rings, help us to understand how rivers behaved in past climates, and place projected climate changes in a broader perspective. While this knowledge is valuable, streamflow reconstructions have not been used to directly inform water management models, because tree rings are annual while water system models require streamflow data of higher resolutions, such as monthly, weekly, or even daily. In our study, we make use of a rich network of tree ring data, consisting of both ring width and stable oxygen isotope ratio, to reconstruct monthly river discharge at four key gauging stations that represent the four main tributaries of the Chao Phraya River, Thailand, thus bridging the gap between tree rings and water management. Our reconstructions, spanning 254 years (1750–2003), are the first monthly streamflow reconstructions outside North America, and the first ones that combine tree rings and oxygen isotope data. Importantly, the reconstructions provide a detailed accounting of past droughts, pluvials, and wet season timings. This added knowledge and data could be used to inform water management decisions, such as the operation of large freshwater impounds supplying hydropower and irrigation water. This functional data set is a significant improvement over conventional annual reconstructions.

1 Introduction

Tree rings, with annual resolution and precise dating, can provide temporally high-resolution proxy records of several climate parameters. However, the annual resolution of tree ring data still restricts how tree-ring-based paleoclimate reconstructions can be used in downstream applications where finer time steps are desirable. Tree-ring-based reconstructions are often compared against historical events, but these comparisons are at times mismatched: while the reconstruction may target one discreet season or the entire year, the event of interest was recorded in another season entirely, that is not captured by the reconstruction. This may result in what Wise (2021) describes as the "seasonal bias". In addition, and specific to water resources, tree ring-based reconstructions of streamflow have provided important insights into surface water availability, but cannot be used directly in water management models which require monthly, weekly, or even daily resolution (Galelli et al., 2021).

How do we obtain subannual climate reconstructions from annual tree rings? Earliest attempts used statistical methods to disaggregate each annual value to multiple subannual ones, assuming a fixed relationship between the two resolutions (Prairie et al., 2007, 2008; Saito et al., 2015; Sauchyn & Ilich, 2017). Later works incorporated multiple species and sites, leveraging the fact that different tree species have different seasonal sensitivities to the hydroclimate, and that there can be different time lags in hydrologic responses at various sites (Stagge et al., 2018; Stahle et al., 2020; Wise, 2021). A third approach uses intra-annual measurements of stable oxygen isotope ratio (δ^{18}O) in tree ring cellulose to reconstruct intra-annual precipitation (Xu et al., 2016, 2021). This approach is very promising, but at its current state the analysis is time-consuming and expensive. Recently, we (Nguyen et al., 2021) proposed a novel modelling framework, called mass balance regression (MBR), that addressed two remaining challenges: to combine proxies optimally for different targets (months or seasons), and to preserve the annual mass balance, ensuring that the subannual flows sum up closely to the annual flow. This framework produced a skillful seasonal reconstruction (wet and dry seasons) for the Ping River, a tributary of the Chao Phraya, Thailand. Importantly, MBR reduced mass imbalances by 45% while maintaining or improving skills compared to ordinary linear regression.

This letter presents a follow-up and extension of that work. Using MBR, we produce a monthly streamflow reconstruction for all four main tributaries of the Chao Phraya, a significant improvement in both temporal resolution and spatial coverage. This is the first monthly streamflow reconstruction outside North America, and the first one that combines ring width and stable oxygen isotope ratio (δ^{18}O). This record reveals the spatiotemporal variability of streamflow, especially monsoonal peak flow timing, over 254 years (1750–2003) across the Chao Phraya River Basin, the most important economic region in Thailand. Importantly, this added knowledge is crucial for water management in the Chao Phraya, where freshwater availability is a limiting factor for many socioeconomic sectors.

2 Materials and Methods

2.1 Study Site and Streamflow Data

The Chao Phraya Basin (Figure 1) is Thailand's most important economic region, serving the country's agricultural and electricity needs with 1.45 million hectares of irrigated land (Divakar et al., 2011) and 3.8 GW of electricity generation capacity from both thermal and hydroelectric sources (Chowdhury et al., 2021). The basin has a dominant monsoon climate. The wet season generally spans from early May to late October, but monsoon rain timing varies year-to-year due to interactions with the El Niño Southern Oscillation (ENSO) and other drivers. El Niño events tend to shorten the rain

season, while La Niña events tend to bring more abundant precipitations (B. I. Cook & Buckley, 2009).

The Chao Phraya has four main tributaries, for each of which we obtained streamflow data from the station with the longest available record. The stations and tributaries are: station P.1 (Ping River), W.4A (Wang River), Y.17 (Yom River), and N.1 (Nan River (Figure 1). Streamflow data at P.1 was naturalized and published by Nguyen et al. (2021) to remove the effect of an upstream reservoir, and this naturalized record was also used here. Data for other stations were obtained from the Thai Royal Irrigation Department (`https://www.hydro-1.net`). With these four stations we aim to capture the spatial variability of streamflow across the basin.

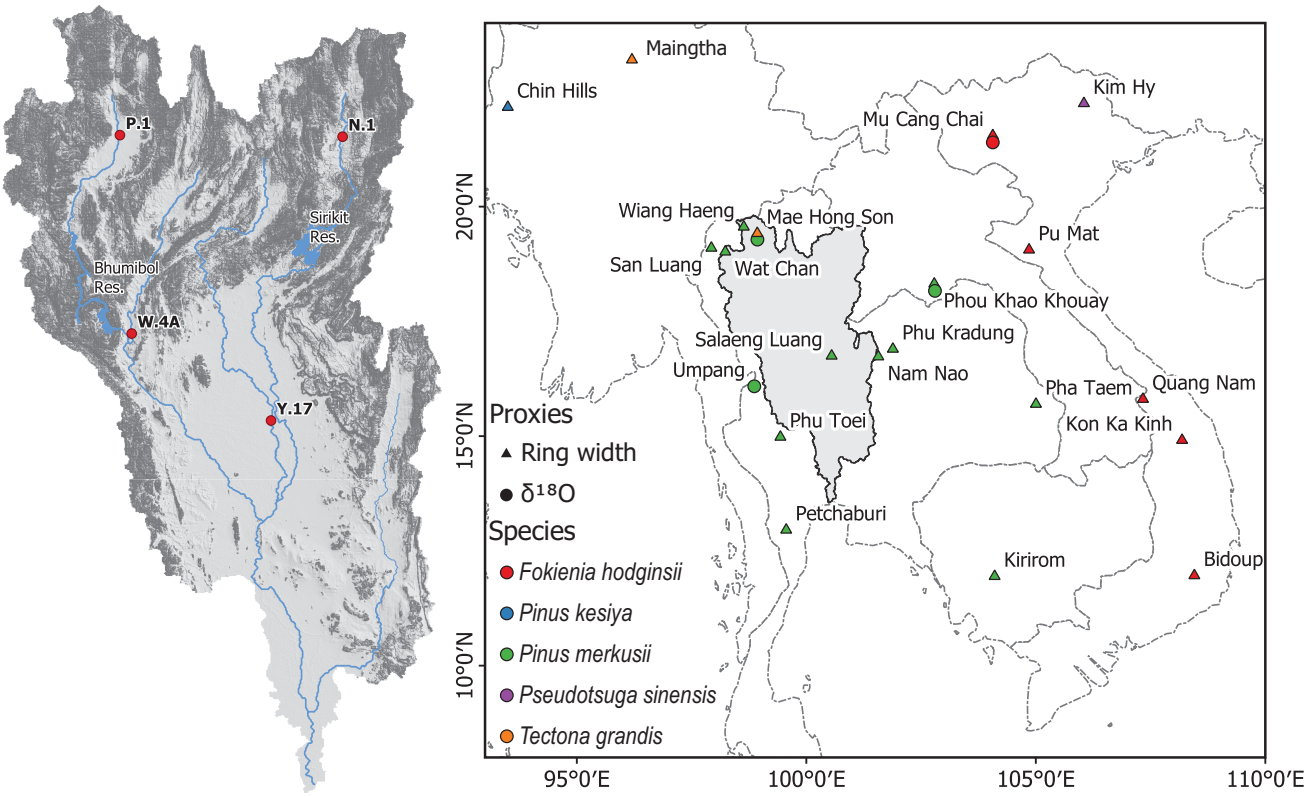

Figure 1. a) Map of the Chao Phraya River Basin, showing the main tributaries, the largest reservoirs (Bhumibol and Sirikit), the streamflow gauges selected for reconstruction, and the topography (mountainous areas in darker shades). b) Locations of the tree ring sites in Southeast Asia used in this study. The location of the Chao Phraya Basin is also shown.

Our proxy data consist of 20 chronologies of ring width and four chronologies of stable oxygen isotope ratio (δ^{18}O) from the Southeast Asia Dendrochronology Network (Figure 1). These are the same chronologies that were used by Nguyen et al. (2021). In that earlier work, we found that our tree ring width chronologies were generally more sensitive to the dry season flow than they were to the wet season flow, while the δ^{18}O chronologies were more sensitive to the wet season flow than they were to the dry season flow (Nguyen et al., 2021, Figure 2). This is the basis for combining them to obtain subannual reconstructions. Interestingly, the δ^{18}O chronologies were also the dominant predictors for the dry season flow (Nguyen et al., 2021, Figure 6), because correlations between dry season flow and δ^{18}O, while smaller in magnitude than those between wet

season flow and δ^{18}O, were still higher than correlations between dry season flow and ring width in many cases. Those findings corroborate the strong amount effect exhibited by δ^{18}O in Thailand and northern Vietnam that were reported earlier (e.g., Sano et al., 2012; Xu et al., 2015, 2019), and demonstrate the value of adding δ^{18}O as a new proxy beside tree ring width. Banking on earlier results, here we use the same proxy network but striving for a higher temporal resolution and a larger spatial coverage.

2.2 Reconstruction Model

The core methodology is the Mass Balance Regression framework (MBR; Nguyen et al., 2021), which was tested for a seasonal resolution earlier, and used here for the first time to achieve a monthly resolution. The two key ideas are: (1) preserve the annual mass balance, that is, ensuring that the sum of the monthly flows matches the annual flow closely, and (2) find the optimal combination of proxies that achieves (1). The essences of the method are as follows. Supposed we have the predictors $\mathbf{X_1}$ for January streamflow $\mathbf{y_1}$, $\mathbf{X_2}$ for February streamflow $\mathbf{y_2}$, and so on. We also have predictors $\mathbf{X_a}$ for the annual flow $\mathbf{Y_a}$. Altogether there are thirteen reconstruction models, which can be merged into one as follows. Let

$$\mathbf{y} = \begin{bmatrix} \mathbf{y_1} \\ \dots \\ \mathbf{y_{12}} \\ \mathbf{y_a} \end{bmatrix}, \quad \mathbf{X} = \begin{bmatrix} \mathbf{X_1} & & & \\ & \dots & & \\ & & \mathbf{X_{12}} & \\ & & & \mathbf{X_a} \end{bmatrix}. \tag{1}$$

We can then form the regression equation

$$\mathbf{y} = \mathbf{X}\boldsymbol{\beta} + \boldsymbol{\varepsilon} \tag{2}$$

where $\boldsymbol{\beta} = [\boldsymbol{\beta_1}, ..., \boldsymbol{\beta_{12}}, \boldsymbol{\beta_a}]'$ are the regression coefficients for the thirteen reconstructions, and $\boldsymbol{\varepsilon}$ is white nose. Equation 2 is solved by least squares:

$$\min_{\boldsymbol{\beta}} \quad J_0 = (\mathbf{y} - \mathbf{X}\boldsymbol{\beta})'(\mathbf{y} - \mathbf{X}\boldsymbol{\beta}), \tag{3}$$

which simultaneously yields thirteen reconstruction models. These models are independent of each other, thus there is no guarantee that the sum of the monthly flows would match the annual flow. To achieve that, we calculate the mass difference

$$\boldsymbol{\delta} = \sum_{i=1}^{12} \mathbf{X_i}\boldsymbol{\beta_i} - \mathbf{X_a}\boldsymbol{\beta_a} \tag{4}$$

and formulate the following *penalized least squares* problem

$$\min_{\beta} \quad J = (\mathbf{Y} - \mathbf{X}\boldsymbol{\beta})'(\mathbf{Y} - \mathbf{X}\boldsymbol{\beta}) + \lambda\boldsymbol{\delta}'\boldsymbol{\delta}. \tag{5}$$

Just as we minimize the squared differences between prediction and observation, we also minimize the squared mass differences $\boldsymbol{\delta}'\boldsymbol{\delta}$. In equation 5, we also introduce the weight λ, which represents the importance of the penalty term: the higher λ is, the more important mass balance becomes. Equation 5 has an analytical solution:

$$\boldsymbol{\beta} = (\mathbf{X}'\mathbf{X} + \lambda\mathbf{A}'\mathbf{A})^{-1}\mathbf{X}'\mathbf{y} \tag{6}$$

where $\mathbf{A} = [\mathbf{X_1} \quad ... \quad \mathbf{X_{12}} \quad -\mathbf{X_a}]$.

As Nguyen et al. (2021) discussed in great detail, the choice of λ is somewhat subjective, depending on the analyst's own priority between model skills and mass balance. As such, we compared the cross-validated reconstruction skills and mass balance with incremental λ values, and chose an appropriate one for each station.

Equation 5 also provides a basis for proxy selection. Each subset p of all chronologies yields one penalized least squares value $J(p)$. Thus we can find the optimal subset of p over all subsets. This can be done with any suitable combinatorial optimization method. Here we used Genetic Algorithms (Holland, 1975; Whitley, 1994). For full details of MBR, including mathematical derivations and proofs, please refer to Nguyen et al. (2021). MBR code is publicly available in the R package `mbr` (Nguyen, 2021).

2.3 Model Evaluation

We assessed the reconstructions using the contiguous leave-k-out cross-validation scheme. In each cross-validation run, a random, contiguous block of k data points was left out, and the model is calibrated on the remaining data. Here k was set as 25% of the data length. The procedure is repeated 50 times. For this monthly reconstruction exercise, it is important that entire years are withheld, that is, the same k data points are withheld from all thirteen reconstruction models (January to December, plus annual). Otherwise, the reconstruction may inadvertently benefit from data leakage, when some months of the year are available in calibration, giving the model partial information about the other months.

The reconstruction was evaluated with the following metrics: coefficient of determination (R^2), reduction of error (RE), and Nash-Sutcliffe coefficient of efficiency (CE) (Fritts et al., 1971; Nash & Sutcliffe, 1970), all of which are commonly used in dendroclimatic reconstructions. These metrics are calculated on the full monthly flow time series, the time series of each month's flow, and the annual flow time series. The formulae for RE and CE are as follows:

$$RE = 1 - \frac{\sum_{i \in \mathcal{V}} (Q_i - \hat{Q}_i)^2}{\sum_{i \in \mathcal{V}} (Q_i - \overline{Q}_c)^2}, \tag{7}$$

$$CE = 1 - \frac{\sum_{i \in \mathcal{V}} (Q_i - \hat{Q}_i)^2}{\sum_{i \in \mathcal{V}} (Q_i - \overline{Q}_v)^2}. \tag{8}$$

Here, $\mathcal{V}$ is the validation set, Q_i the observed flow at time i, $\hat{Q}_i$ the reconstructed flow at time i, $\overline{Q}_c$ the mean streamflow over the calibration set, and $\overline{Q}_v$ the mean streamflow over the validation set. Essentially, these metrics normalize the model's sum of squared error against that of a benchmark model, one that uses the mean over the calibration period in the case of RE, and mean over the validation period in the case of CE.

2.4 Droughts, Pluvials, and Monsoon Flow Timing

From the monthly reconstructions, we calculated the Standardized Streamflow Index (SSI; Shukla & Wood, 2008), which has the same formulation as the Standardized Precipitation Index (SPI; McKee et al., 1993) and the Standardized Precipitation-Evapotranspiration Index (SPEI; Vicente-Serrano et al., 2010), except that streamflow is the input. Similarly to the other two indices, SSI can be calculated at multiple time scales, such as 1-month (SSI_1), 6-month (SSI_6), and 12-month (SSI_{12}); these calculations are only possible with monthly reconstructions. SSI is calculated as follows. First, streamflow is converted to rolling averages at the desired window (e.g., 6-month). Then, a log-logistic distribution is fitted to the new time series to obtain a non-exceedance probability for each value. Finally, a standardized index is obtained by applying the inverse standard normal cumulative density function to the probabilities. These calculations were carried out using the R package `SPEI` (Beguería & Vicente-Serrano, 2017).

Converting streamflow to a standardized index allows us to make comparisons across four rivers, thereby providing a basis for assessing droughts and pluvials. Our working definition for droughts and pluvials are as follows. A drought starts with two consecutive months of negative SSI, and ends with two consecutive months of positive SSI (the

last two positive months do not count towards its duration). The SSI sign is reverse for pluvials. Thus a sequence of alternating positive and negative SSI (e.g., -1 +1 -1 +1) can be either a part of a drought, a pluvial, or neither.

Finally, we explored how the timing of the monsoon flow season changed over time. We adopted the season delineation method of B. I. Cook and Buckley (2009). The curve of cumulative flow over time was derived for each year. Onsets and withdrawals were then determined based on change points in the slope of the curve: a change from mild to steep slope marks the onset of the monsoon flow season, and a change from steep to mild slope marks the withdrawal. These change points were detected using two-phase linear regression (Lund & Reeves, 2002), a method commonly used with meteorological time series. Two-phase linear regression is usually done with daily time series, and we adapted it for monthly time series here.

3 Results and Discussion

3.1 Reconstruction Performance

We first compare the reconstructed monthly time series at each station against the corresponding instrumental time series (Figure 2a). All reconstructions match well with the instrumental data. R^2, RE, and CE values range between 0.74 and 0.91. The seasonal patterns are also well reproduced. Overall, streamflow variability and seasonality are very well captured by the tree ring records and the reconstruction model. However, the reconstructions are not perfect, and closer examinations reveal three limitations that provide interesting and important insights for future development in high-resolution dendrohydrology.

First, we found that peak flow in the wettest years were under estimated, e.g., Nan River's flow in 1940 and 1941, and Ping River's flow in 1971 and 1973 (Figure 2a). Peak flow underestimation is commonly observed in tree-ring-based reconstructions (see e.g. Robeson et al., 2020). There are two possible reasons. First, the relationship between tree ring proxies and streamflow may become nonlinear at the extremes (Torbenson & Stagge, 2021). Second, a main flood generation mechanism in Thailand is heavy rain on saturated soil (Lim & Boochabun, 2012; Stein et al., 2020), but streamflow generated by saturation excess overland flow cannot be captured by tree rings. While $\delta^{18}O$ in tree rings is not limited by soil saturation, there are only four δ^{18}O chronologies in our record, limiting the amount of information that can be recovered for peak flows.

Second, in some years, the annual hydrograph has a bimodal shape instead of a single peak, for example Ping River in 1923 and Nan River in 1936 (Figure 2b). In these cases, the first streamflow peak resulted from heavy rains due to tropical cyclones in early summer, and the second peak was generated from monsoon rains. This bimodal shape was not reproduced in the reconstruction. Trees take time to convert moisture into growth of wood cells, and in that process both ring width and δ^{18}O lose some high frequency signals.

The RE and CE values we reported in Figure 2a are higher than typically reported in dendroclimatology. This is because we work with monthly time series with distinct seasonal patterns, while the benchmark used in the RE and CE metrics is the overall mean, which does not contain any seasonality information. Therefore, we conducted a more stringent assessment where the skill metrics were calculated for each month, against the corresponding monthly means (Figure 2c). In some cases we still observed R^2 and RE values about 0.8, but most values are (as expected) lower, in the range of 0.3–0.7. Highest CE values were about 0.6, while most are in the range of 0.2–0.4. Notably, negative CE occurred for February (Ping River) and March (Yom River). This reveals the third limitation of the reconstructions. In these driest months the trees are mostly dormant, with none or little growth. Information about flow for these months are likely recovered

more from autocorrelations with other months than from tree rings, leading to the low out-of-sample predictive skills in these months.

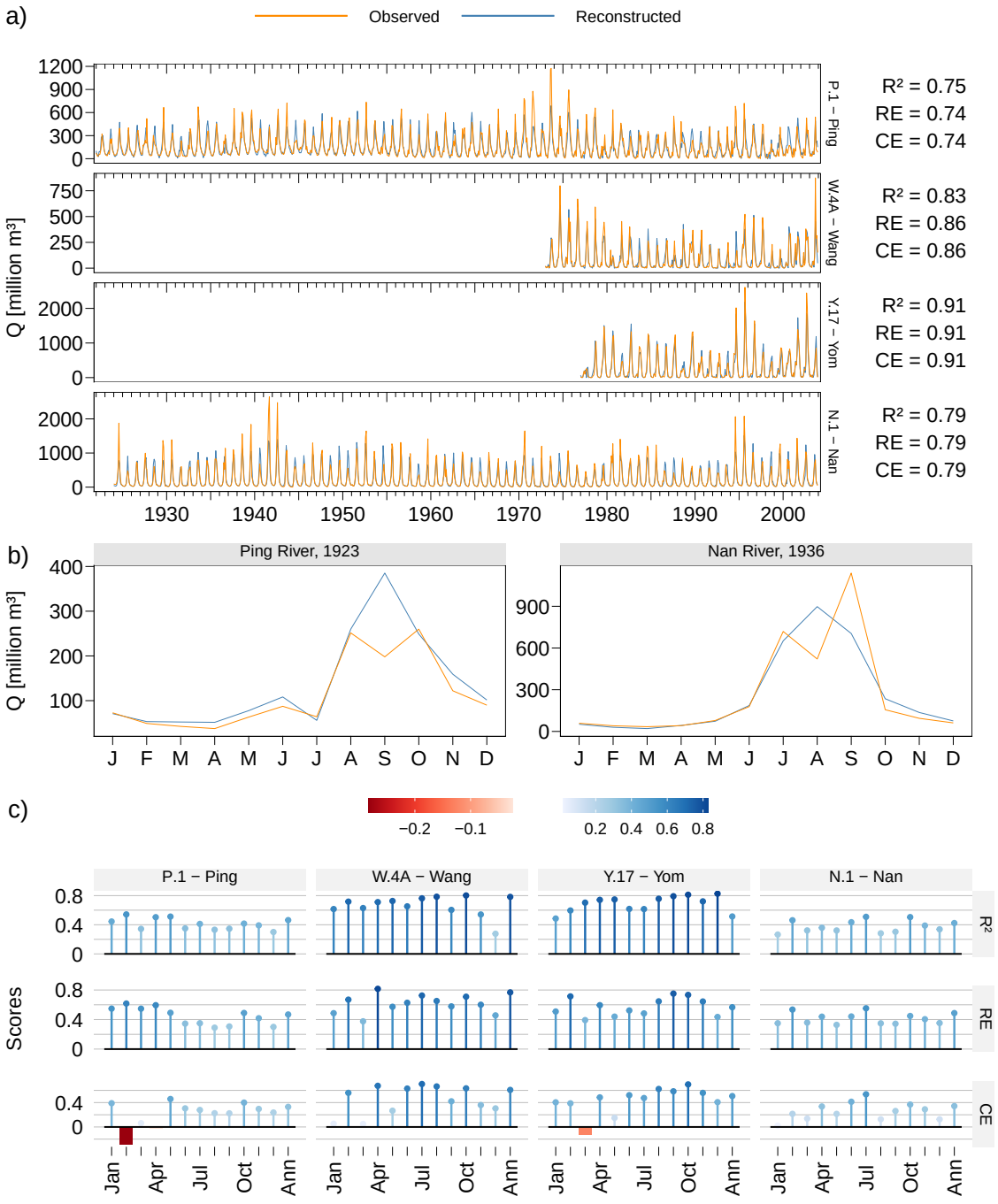

Figure 2. a) Comparison of the reconstructed and instrumental monthly flow, and the overall skill scores. b) Examples of years that have two peaks in the hydrograph which were not captured well by tree rings. c) Individual skill scores of thirteen reconstruction models (January–December, and annual) for each station.

These limitations occurred only in special cases. Overall, the reconstructions have acceptable to very good skills. There are several interesting research directions that can help overcome the limitations that we pointed out here. First is the use of nonlinear methods (e.g. Nguyen & Galelli, 2018; Torbenson & Stagge, 2021) to account for nonlinearities in the streamflow–proxy relationship at the extremes. Second, development of more δ^{18}O chronologies is needed for the region, as δ^{18}O have been shown to capture well hydrological extremes (Xu et al., 2019; An et al., 2022). Particularly, intra-annual δ^{18}O chronologies similar to those developed recently in China (Xu et al., 2016, 2021) would be valuable for high-resolution reconstructions in Southeast Asia. Third is the development of more tree ring chronologies in general, so as to enhance the signals contained in the tree ring network. The number of tree ring chronologies in the tropics is much lower than that in temperate regions.

3.2 Droughts and Pluvials

We calculated 1-month, 6-month, and 12-month SSI from the reconstruction for each river. Here, we discuss the results related to SSI_6 (Figure 3), and results for other indices, together with the raw monthly streamflow time series, are shown in Figures S1–S4. SSI_6 represents the seasonal time scale of droughts and pluvials.

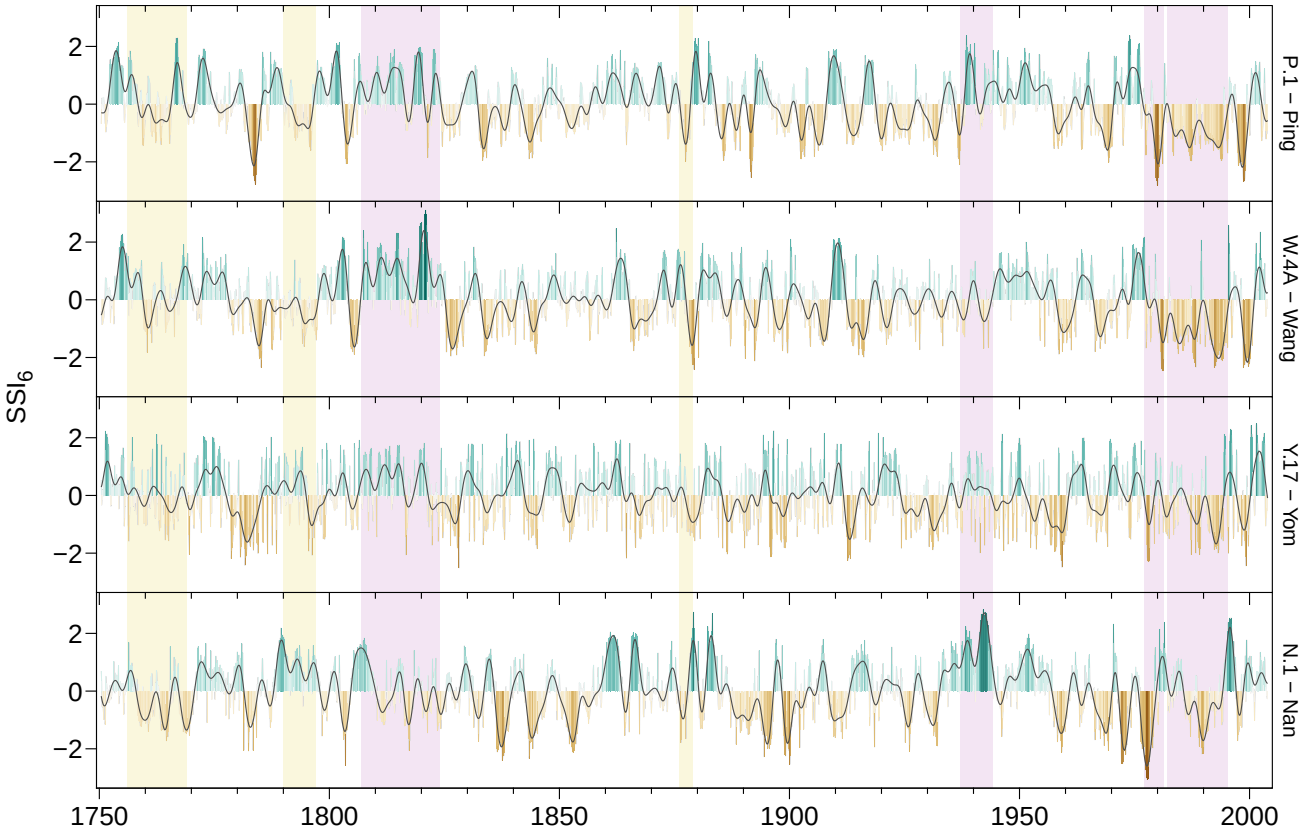

Figure 3. Monthly time series of 6-month standardized streamflow index (SSI_6) for each river, colored in brown and teal. The black lines show 3-year low-pass filtered time series. Highlighted in yellow are the megadroughts reported by E. R. Cook et al. (2010), namely the Strange Parallels Drought (1756–1768), East India Drought (1790–1796), and Victorian Great Drought (1876–1878). Other droughts and pluvials discussed in the text are highlighted in violet.

In the Ping and Wang Rivers (the two western tributaries), we note a common prolonged dry period between 1982–1995 that stands out across the full time series. This period consists of two consecutive droughts. In the Ping River, the droughts lasted from 01/1982–05/1985 (77 months) and from 09/1988–04/1994 (68 months); these are the two longest droughts in the Ping record. In the Wang, the droughts lasted from 11/1982–02/1987 (52 months) and 01/1990–04/1995 (64 months); these droughts rank third and first among all droughts at this station in terms of duration. The two eastern tributaries (Yom and Nan) also experienced a dry period during these times, but droughts are less prominent. Almost immediately before the 1982–1995 droughts were another that was shorter but more severe. Peak SSI_6 values of -2.81 in December 1979 at P.1, -2.46 in March 1981 at W.4, and -3.05 in October 1977 at N.1 were the lowest SSI_6 in the whole record at each station, respectively. Another notable drought occurred around 1780–1786 that affected all four tributaries, but streamflow reduction was less severe in the Nan compared to the other three rivers.

In the reconstruction we also found the footprints of the post-1750 megadroughts that E. R. Cook et al. (2010) reported, namely the Strange Parallel Droughts (1756–1768), the East India Drought (1790–1796), and the Victorian Great Drought (1876–1878). Each megadrought was expressed differently in each tributary. The Strange Parallels was most severe in the Nan River. The East India Drought led to moderately dry conditions in the Ping and Wang, and a mix of wet and dry periods in the Yom, but curiously it was not felt in the Nan at all.

There are notable pluvials as well, particularly between 1807–1823 at W.4A, when a series of pluvials occurred, including the wettest one in the record. Each pluvial lasted between 10–45 months, interspersed with two-to-three-month bursts of mildly dry conditions. This wet period is also seen in the Ping and Yom Rivers, but not in the Nan. Contrarily, the Nan went through a prominent pluvial between 04/1937–04/1944. Lasting 85 months with a peak SSI_6 of 2.82, this is the wettest and second longest among all pluvials in our record. Interestingly, in all four rivers we observe clusters of pluvials, but the frequencies of these clusters appearing are different among the tributaries. Episodic floodplain stripping has been documented on the Ping River, by a geomorphic and morphostratigraphic analysis by Wasson et al. (2021). These events were caused by extreme floods, or clusters of extreme floods, the last being a single flood in 1831. This flood was captured by our reconstructions: September 1831 was the seventh highest monthly flow among 3,048 months of record (Figure S2 and Code S1).

Overall, the reconstruction shows both similarities and differences in the drought and pluvial histories of the four rivers. There is a degree of coherence: droughts and pluvials often occur in more than one tributary. But there is also spatial heterogeneity: there are differences in magnitude and timing of events across the tributaries, and few events affect all four.

3.3 Wet Season Onset

We used the method of B. I. Cook and Buckley (2009) to determine the onset and withdrawal timing of the wet season in each year (Section 2.4). We also calculated the z-score of the total annual flow to determine whether each year was dry ($z < 0$; low total flow) or wet y($z > 0$; high total flow). The procedure was applied to each tributary separately. We found that the withdrawal month was always the same: October, but the onset months varied between May and September (Figure 4a). For the Ping, 137 years (54%) have onset in July, 76 years (30%) in May or June, and 41 years (16%) in September. Onsets tend to be later in the Wang and Yom Rivers compared to the Ping, with 55–60% occurred in August, while the months between May–July each shares about 8–15% of the distribution. Another 8% of the Yom's wet season started in September. In

stark contrasts to these three tributaries, the Nan's wet season almost exclusively begin in July; in only four years (2%) was onset occurred in June.

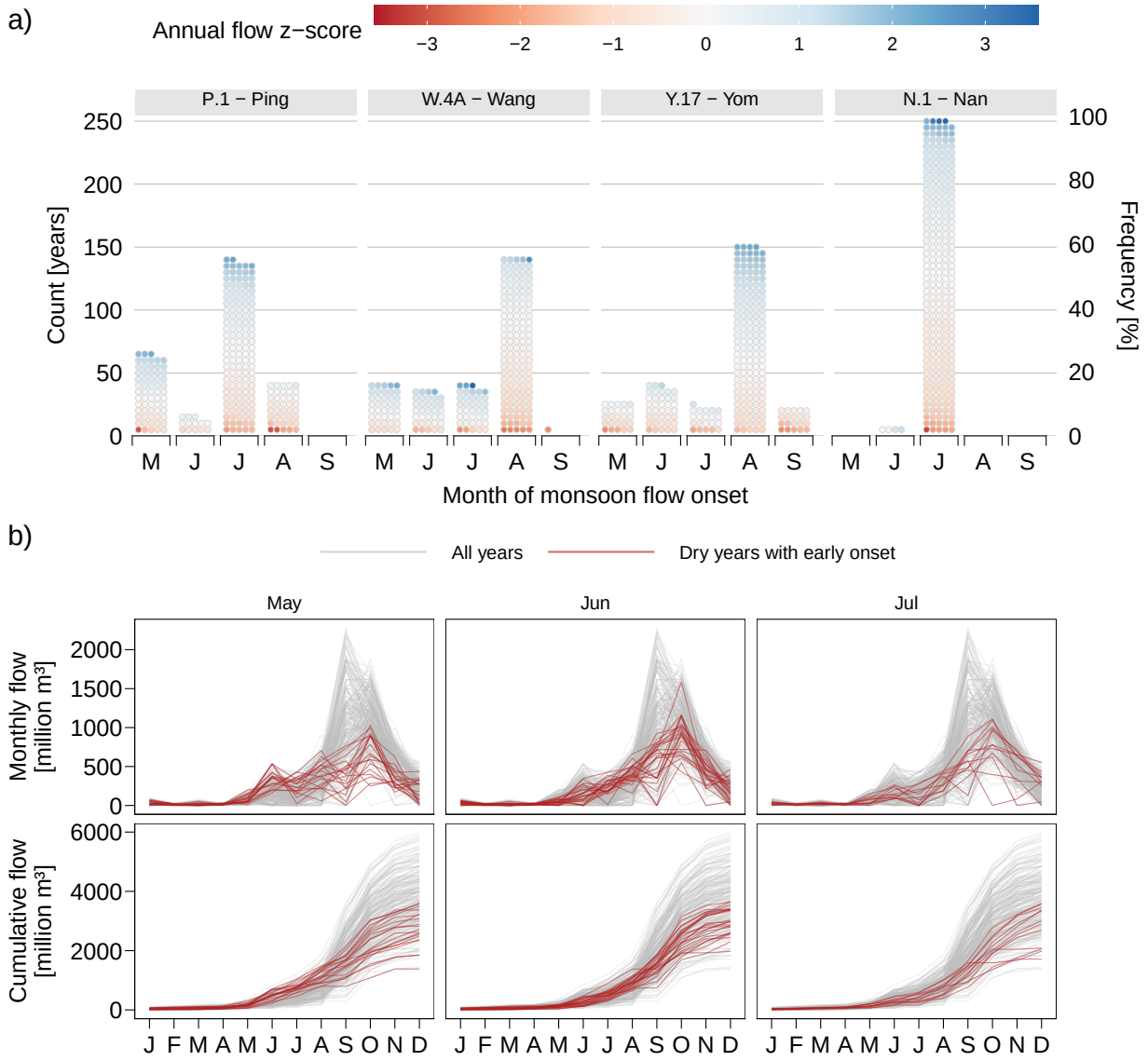

Figure 4. a) Histograms of wet season onset timing (month). Each bar contains a number of stacked dots which is the number of years having the same onset month, from April to September. Each dot is colored by the z-score of the total annual flow. Thus the color distribution in each bar tells whether years having onset in that month would be more likely to have high flow (more blue dots) or low flow (more red dots). b) Annual hydrographs (first row) and cumulative flow curves (second row) of station Y.17 on Yom River. The grey lines show all 254 years in the reconstruction. The red lines highlight the years with early wet season onset but low total annual flow; each column highlights the years with onsets in the corresponding month.

For the Ping, years with onset between May–July are slightly more likely to be wet (55% of the time) while years with late onset (August) are more likely to be dry (73%).

Similarly, wet seasons that start in May–July in the Wang are more likely to produce high annual flows (65–70% of the time) while those starting in August tend to produce low flow (63% of the time). These patterns make intuitive sense. Counter-intuitive is the Yom River: early onsets (May–July) are less likely to produce high total flow ($z > 0$ in only 24-43%) than those in August (64%), yet onsets in September always produced dry years. To seek an explanation for this curious case, we explore the annual hydrographs and the cumulative flow curves of this river (Figure 4b). The hydrographs of the Wang River at Y.17 have prominent peaks in June, more so than the other tributaries. This is because Y.17 is located in the lowlands and is not shielded from early summer tropical typhoons like the other three stations that are surrounded by mountains. Consequently, this area receives more typhoon rain, leading to higher June flows. Interestingly, years with the highest June flows are associated with lower peak flows, causing a slope change in May for the cumulative flow curve (Figure 4b, first column). This effect is also observed with slope changes in June and July (Figure 4b, second and third columns). More research is needed to determine the mechanism behind this behavior. If the association between higher summer flow and lower peak flow can be further verified, it would equip irrigation planners with a better forecasting tool, as a more robust estimation of peak flow distribution could then be obtained based on the summer flow.

The unique distribution of wet season timing at N.1 could also be explained with the same mechanism concerning typhoon rain. N.1 is located further most inland, surrounded by mountains (Figure 1), thus shielded from early summer typhoon rain. As a result, the hydrograph of N.1 is much more homogeneous from year to year. Streamflow in the Chao Phraya is generated from both typhoons and monsoon rains. Each subcatchment is exposed differently to these sources due to its location and topography. The interaction between the moisture sources and catchment characteristics lead to the spatiotemporal variability of wet season timing.

4 Conclusions

Using a network of 20 ring width and four $\delta^{18}O$ chronologies, we produce 254-year, monthly resolved reconstructions of streamflow for four major tributaries of the Chao Phraya, Thailand. The reconstructions have very good skills in capturing streamflow variability, except for the driest months (February and March), the wettest years, and some years with two hydrograph peaks. Our reconstructions provide a detailed record of streamflow variability, showing both coherence and heterogeneity of droughts and pluvials across the Chao Phraya Basin. Owing to the monthly resolution, our reconstructions also reveal how wet season timing has varied. Rainfall supply to wet season flow comes from tropical typhoons and monsoon rains, the interactions between which create the spatial and temporal variability of wet season timing.

These results are particularly important when seen through the lens of water management. The Chao Phraya is water-stressed: freshwater availability *per capita* is about 2,230 m^3/year (Divakar et al., 2011; World Bank, 2011), less than the national average (3,244 m^3/year) and only 39% of the world's average (5,732 m^3/year) (FAO, 2017). Worse still, water availability is not constant throughout the year, as the monsoon brings stark contrasts to the annual hydrograph. Our monthly reconstruction could be used to operate the Chao Phraya water system better. For example, it could help coordinate the operations of Thailand's two largest reservoirs—Bhumibol and Sirikit—both of which are in the Chao Phraya, to mitigate concurrent floods or droughts while meeting irrigation and hydropower demands, which vary greatly from month to month (Divakar et al., 2011). With monthly-resolved reconstructions, we have partly bridged the gap between what tree rings can offer and what water management needs.

5 Open Research

All data and code used in this project is available on GitHub at `https://github.com/ntthung/chao-phraya-monthly` (DOI: 10.5281/zenodo.6830888). On the GitHub repository we provide a document that details the step-by-step workflow with code, discussion, as well as all intermediate and final results. This document is also included in the Supporting Information (Code S1). The reconstructions will be uploaded to the International Tree Ring Data Bank if the paper is accepted. All analyses were conducted using the open source R statistical computing environment.

Acknowledgments

We are indebted to the helpful comments and suggestions by Robert Wasson and Lim Han She. Hung Nguyen is supported by the Lamont-Doherty Earth Observatory Postdoctoral Fellowship; part of this work was conducted while he was a PhD student supported by the Singapore University of Technology and Design President's Graduate Fellowship. Chenxi Xu is supported by the National Natural Science Foundation of China, Grant Number: 42022059, 41888101; the Chinese Academy of Sciences (CAS) Pioneer Hundred Talents Program, the Strategic Priority Research Program of the Chinese Academy of Sciences, Grant Number: XDB26020000, and the Key Research Program of the Institute of Geology and Geophysics (CAS Grant IGGCAS-201905). Brendan Buckley is supported by the US National Science Foundation grants AGS-1602629 and AGS-2001949. We acknowledge computing resources from Columbia University's Shared Research Computing Facility project, which is supported by NIH Research Facility Improvement Grant 1G20RR030893-01, and associated funds from the New York State Empire State Development, Division of Science Technology and Innovation (NYSTAR) Contract C090171, both awarded April 15, 2010. We also acknowledge computing support from the Singapore National Super Computing Centre for the initial phase of this project.

References

An, W., Li, J., Wang, S., Xu, C., Shao, X., Qin, N., & Guo, Z. (2022). Hydrological Extremes in the Upper Yangtze River Over the Past 700 yr Inferred From a Tree Ring δ18O Record. *Journal of Geophysical Research: Atmospheres*, *127*(10), e2021JD036109. doi: 10.1029/2021JD036109

Beguería, S., & Vicente-Serrano, S. M. (2017). *SPEI: Calculation of the standardised precipitation-evapotranspiration index* [Manual].

Chowdhury, A. F. M. K., Dang, T. D., Nguyen, H. T. T., Koh, R., & Galelli, S. (2021). The Greater Mekong's Climate-Water-Energy Nexus: How ENSO-Triggered Regional Droughts Affect Power Supply and CO2 Emissions. *Earth's Future*, *9*(3), e2020EF001814. doi: 10.1029/2020EF001814

Cook, B. I., & Buckley, B. M. (2009, December). Objective determination of monsoon season onset, withdrawal, and length. *Journal of Geophysical Research*, *114*(D23), D23109. doi: 10.1029/2009JD012795

Cook, E. R., Anchukaitis, K. J., Buckley, B. M., D'Arrigo, R. D., Jacoby, G. C., & Wright, W. E. (2010, April). Asian Monsoon Failure and Megadrought During the Last Millennium. *Science*, *328*(5977), 486–489. doi: 10.1126/science.1185188

Divakar, L., Babel, M., Perret, S., & Gupta, A. D. (2011, April). Optimal allocation of bulk water supplies to competing use sectors based on economic criterion – An application to the Chao Phraya River Basin, Thailand. *Journal of Hydrology*, *401*(1-2), 22–35. doi: 10.1016/j.jhydrol.2011.02.003

FAO. (2017). *AQUASTAT Database.* http://www.fao.org/aquastat/statistics/query/index.html.

Fritts, H. C., Blasing, T. J., Hayden, B. P., & Kutzbach, J. E. (1971, October). Multivariate Techniques for Specifying Tree-Growth and Climate Relation-

ships and for Reconstructing Anomalies in Paleoclimate. *Journal of Applied Meteorology*, *10*(5), 845–864. doi: 10.1175/1520-0450(1971)010⟨0845:MTFSTG⟩2.0.CO;2

Galelli, S., Nguyen, H. T. T., Turner, S. W. D., & Buckley, B. M. (2021, August). Time to Use Dendrohydrological Data in Water Resources Management? *Journal of Water Resources Planning and Management*, *147*(8), 01821001. doi: 10.1061/(ASCE)WR.1943-5452.0001422

Holland, J. H. (1975). *Adaptation In Natural and Artificial Systems.* Ann Arbor, Michigan: The University of Michigan Press.

Lim, H. S., & Boochabun, K. (2012). Flood generation during the SW monsoon season in northern Thailand. *Geological Society, London, Special Publications*, *361*(1), 7–20. doi: 10.1144/SP361.3

Lund, R., & Reeves, J. (2002, September). Detection of Undocumented Changepoints: A Revision of the Two-Phase Regression Model. *Journal of Climate*, *15*(17), 2547–2554. doi: 10.1175/1520-0442(2002)015⟨2547:DOUCAR⟩2.0.CO;2

McKee, T. B., Doesken, N. J., & Kleist, J. (1993, January). The relationship of drought frequency and relation to time scales. In *Eighth Conference on Applied Climatology* (p. 6). Anaheim, California.

Nash, J. E., & Sutcliffe, J. V. (1970, April). River flow forecasting through conceptual models part I — A discussion of principles. *Journal of Hydrology*, *10*(3), 282–290. doi: 10.1016/0022-1694(70)90255-6

Nguyen, H. T. T. (2021, February). *Mbr: Mass-balance Regression. R package version 0.0.1.*

Nguyen, H. T. T., & Galelli, S. (2018, March). A Linear Dynamical Systems Approach to Streamflow Reconstruction Reveals History of Regime Shifts in Northern Thailand. *Water Resources Research*, *54*(3), 2057–2077. doi: 10.1002/2017WR022114

Nguyen, H. T. T., Galelli, S., Xu, C., & Buckley, B. M. (2021). Multi-Proxy, Multi-Season Streamflow Reconstruction with Mass Balance Adjustment. *Water Resources Research*, *57*(8), e2020WR029394. doi: 10.1029/2020WR029394

Prairie, J., Nowak, K., Rajagopalan, B., Lall, U., & Fulp, T. (2008). A stochastic nonparametric approach for streamflow generation combining observational and paleoreconstructed data. *Water Resources Research*, *44*(6), 1–11. doi: 10.1029/2007WR006684

Prairie, J., Rajagopalan, B., Lall, U., & Fulp, T. (2007). A stochastic nonparametric technique for space-time disaggregation of streamflows. *Water Resources Research*, *43*(3), 1–10. doi: 10.1029/2005WR004721

Robeson, S. M., Maxwell, J. T., & Ficklin, D. L. (2020). Bias Correction of Paleoclimatic Reconstructions: A New Look at 1,200+ Years of Upper Colorado River Flow. *Geophysical Research Letters*, *47*(1), 1–12. doi: 10.1029/2019GL086689

Saito, L., Biondi, F., Devkota, R., Vittori, J., & Salas, J. D. (2015, October). A water balance approach for reconstructing streamflow using tree-ring proxy records. *Journal of Hydrology*, *529*, 535–547. doi: 10.1016/j.jhydrol.2014.11.022

Sano, M., Xu, C., & Nakatsuka, T. (2012, June). A 300-year Vietnam hydroclimate and ENSO variability record reconstructed from tree ring δ 18 O. *Journal of Geophysical Research: Atmospheres*, *117*(D12), D12115. doi: 10.1029/2012JD017749

Sauchyn, D., & Ilich, N. (2017, November). Nine Hundred Years of Weekly Streamflows: Stochastic Downscaling of Ensemble Tree-Ring Reconstructions. *Water Resources Research*, 1–18. doi: 10.1002/2017WR021585

Shukla, S., & Wood, A. W. (2008). Use of a standardized runoff index for characterizing hydrologic drought. *Geophysical Research Letters*, *35*(2). doi: 10.1029/2007GL032487

Stagge, J. H., Rosenberg, D. E., DeRose, R. J., & Rittenour, T. M. (2018). Monthly paleostreamflow reconstruction from annual tree-ring chronologies. *Journal of Hydrology*, *557*, 791–804. doi: 10.1016/j.jhydrol.2017.12.057

Stahle, D. W., Cook, E. R., Burnette, D. J., Torbenson, M. C. A., Howard, I. M., Griffin, D., ... Crawford, C. J. (2020, March). Dynamics, Variability, and Change in Seasonal Precipitation Reconstructions for North America. *Journal of Climate*, *33*(8), 3173–3195. doi: 10.1175/JCLI-D-19-0270.1

Stein, L., Pianosi, F., & Woods, R. (2020, March). Event-based classification for global study of river flood generating processes. *Hydrological Processes*, *34*(7), 1514–1529. doi: 10.1002/hyp.13678

Torbenson, M. C. A., & Stagge, J. H. (2021). Informing Seasonal Proxy-Based Flow Reconstructions Using Baseflow Separation: An Example From the Potomac River, United States. *Water Resources Research*, *57*(2), e2020WR027706. doi: 10.1029/2020WR027706

Vicente-Serrano, S. M., Beguería, S., & López-Moreno, J. I. (2010, April). A Multiscalar Drought Index Sensitive to Global Warming: The Standardized Precipitation Evapotranspiration Index. *Journal of Climate*, *23*(7), 1696–1718. doi: 10.1175/2009JCLI2909.1

Wasson, R. J., Ziegler, A., Lim, H. S., Teo, E., Lam, D., Higgitt, D., ... Singhvi, A. K. (2021, February). Episodically Volatile High Energy Non-Cohesive River-Floodplain Systems: New Information from the Ping River, Thailand, and a Global Review. *Geomorphology*, 107658. doi: 10.1016/j.geomorph.2021.107658

Whitley, D. (1994, June). A genetic algorithm tutorial. *Statistics and Computing*, *4*(2). doi: 10.1007/BF00175354

Wise, E. K. (2021). Sub-Seasonal Tree-Ring Reconstructions for More Comprehensive Climate Records in U.S. West Coast Watersheds. *Geophysical Research Letters*, *48*(2), e2020GL091598. doi: 10.1029/2020GL091598

World Bank. (2011, June). *Thailand environment monitor: Integrated water resources management - a way forward* (Tech. Rep. No. 63368). Washington, D.C: World Bank Group.

Xu, C., Buckley, B. M., Promchote, P., Wang, S. Y. S., Pumijumnong, N., An, W., ... Guo, Z. (2019). Increased Variability of Thailand's Chao Phraya River Peak Season Flow and Its Association With ENSO Variability: Evidence From Tree Ring δ18O. *Geophysical Research Letters*, *46*(9), 4863–4872. doi: 10.1029/2018GL081458

Xu, C., Pumijumnong, N., Nakatsuka, T., Sano, M., & Li, Z. (2015). A tree-ring cellulose δ18O-based July-October precipitation reconstruction since AD 1828, northwest Thailand. *Journal of Hydrology*, *529*(P2), 433–441. doi: 10.1016/j.jhydrol.2015.02.037

Xu, C., Zheng, H., Nakatsuka, T., Sano, M., Li, Z., & Ge, J. (2016, June). Inter- and intra-annual tree-ring cellulose oxygen isotope variability in response to precipitation in Southeast China. *Trees*, *30*(3), 785–794. doi: 10.1007/s00468-015-1320-2

Xu, C., Zhu, H., Wang, S.-Y. S., Shi, F., An, W., Li, Z., ... Guo, Z. (2021, September). Onset and maturation of Asian summer monsoon precipitation reconstructed from intra-annual tree-ring oxygen isotopes from the southeastern Tibetan Plateau. *Quaternary Research*, *103*, 139–147. doi: 10.1017/qua.2020.28